AIMS Materials Science, 11(1): 129–149.
DOI: 10.3934/matersci.2024008
Received: 25 October 2023
Revised: 28 December 2023
Accepted: 03 January 2024
Published: 30 January 2024

http://www.aimspress.com/journal/Materials

Research article

Mechanical, fatigue, and superplasticity properties of Cu-Al-Mn, Cu-Al-Be-Mn shape memory alloy and their metal matrix composites

Naresh H.[1], Prashantha S.[1], N.R. Banapurmath[2,*], M.A. Umarfarooq[2], Chandramouli Vadlamudi[3] and Sanjay Krishnappa[3]

[1] Department of Mechanical Engineering, Siddaganga institute of technology, Tumakuru-572103, India
[2] School of Mechanical Engineering, Centre for Material Science, KLE Technological University, BVB Campus, Hubballi 580031, India
[3] Aerospace Integration Engineer, Aerosapien Technologies, Daytona Beach, FL 32114, USA

* **Correspondence:** Email: nrbanapurmath@gmail.com; Tel: +91-9880-726-748.

Abstract: This study explores the characteristics and potential engineering applications of Cu-Al-Mn and Cu-Al-Be-Mn shape memory alloys (SMAs). The research investigates the chemical composition, transformation temperatures, and mechanical properties of these SMAs when incorporated into Al metal matrix composites. It was found that the addition of Mn and Be has a significant impact on the performance of Cu-Al alloys. Among Cu-Al-Mn SMAs, SMA 1, with a composition of Cu-80.94%, Al-10.54%, and Mn-8.52%, exhibited superior strain recovery, super elasticity (SE), and improved mechanical properties compared to other compositions. The study also demonstrates that the inclusion of SMA fibers in Al composites enhances residual strength, energy absorption capacity, and the ability to close fissures, contributing to a more robust and resilient material. In the case of Cu-Al-Be-Mn SMA (SMA 6) with Cu-87.42%, Al-11.8%, Be-0.48%, and Mn-0.3%, displayed improved properties, outperforming other compositions in terms of strain recovery, residual strength, energy absorption capacity, and crack-closing ability. These findings suggest that Cu-Al-Be-Mn SMAs hold promise for various engineering applications. The study provides valuable insights into the potential of these SMAs to enhance the performance of structural materials, offering increased strength, ductility, and resilience. This research contributes to a deeper understanding of the applications and advantages of SMAs in the field of engineering.

Keywords: Cu-Al-Mn SMA; shape recovery; residual strength; crack strength; energy absorption capacity; metal matrix composites

1. Introduction

Smart materials have the remarkable ability to sense and are widely utilized in various sectors like robotics, structural engineering, biomedicine, and aerospace technology. Within the realm of smart materials, shape memory alloys (SMAs) stand out due to their distinctive features. They can return to their original shape after deformation, achieved either through changes in temperature (known as the shape memory effect (SME)) or by relieving applied stress (referred to as pseudo elasticity) and retention of SME even after extensive mechanical cycling. Super elasticity (SE) and SME set SMAs apart as smart materials with exceptional capabilities. SE is the capacity to recover to a predetermined shape after experiencing significant nonlinear deformation. In simpler terms, after the applied stress is removed, any inelastic distortion occurring beyond the austenite completion temperature (Af) can promptly revert to its initial state. This suggests that after unloading, inelastic deformation persists but recovers when the alloy is heated to a temperature above Af. Since their creation in the 1960s, the SMAs have mostly been utilized in the fields of medical, aeronautical, and automotive engineering [1–4].

The concept of SME was first observed by Chang and Read in the case of an Au-Cd alloy approximately in 1951. Subsequently, in 1953, a similar effect was reported in an In-Tl alloy [5]. It wasn't until 1962 that William J. Buehler discovered a remarkable SMA, which he aptly named "Nitinol" as a tribute to the Naval Ordnance Laboratories. This alloy exhibited excellent strain recovery properties and demonstrated remarkable thermal stability [6]. The use of SMAs in the fields of architectural and civil engineering has recently been expanded. Controlling oscillations brought on by outside forces like winds, earthquakes, and traffic is especially important for buildings and bridges because they can lead to progressive failure and damage [7–9]. SMAs in the wire form and plates have been utilized to control the behavior of the structural components and to offer resistance to the external loads. The energy loss, secant stiffness, residual strain, and equivalent damping of the SMA wires were investigated by Dolce and Cardone [10,11] using tensile testing and cyclic torsion. Results demonstrated that the SMA wires had a significant capacity for energy dissipation and fatigue resistance, making them an excellent choice to utilize as seismic devices. Using SMA's super elastic and damping properties, Mekki and Auricchio [12] proposed an energy dissipation machine for cables in cable-stayed bridges. They evaluated the impact of the SMA device's area, length, and location on the ability to regulate cable movement.

Torra et al. [13] examined the effectiveness of SMA wire dampers in stayed cables and included recommendations for the quantity and length of SMA wires that should be used. SMA wire dampers were suggested by Zhang and Zhu [14] as a means of regulating a three-story building's seismic reaction. The suggested dampers of SMA for the dissipation of large energy during earthquakes use an SMA wire. To improve the seismic performance of structures, deformation control machines such as connections, braces, and base isolators were suggested in addition to dampers [15–18].

Pre-stressing or strengthening of concrete and structural elements has been the subject of studies [19–21]. An experimental investigation was undertaken by Abdulridha and Palermo [22] to evaluate the enactment of an SMA steel-reinforced concrete thin shear wall that demonstrated significant displacement restitution after being subjected to significant drifts. A promising method for

strengthening the walls of old buildings was developed by Branco et al. [23] by using the hysteretic behavior of the wires to reinforce a composite wall. For strengthening reinforced concrete structures, Shahverdi et al. [24] exploited the iron-based SMA strips, which emerge from recovery stress due to their mechanical fixation, and reported enhancement of SMA's use and functionality in cement-based members. Beam specimens with dimensions of 160 mm in length and 40 mm in width were created. SMA fibers were dispersed at random with cementitious components. The SMA fiber-reinforced cement composites were then solely applied to the bottom of the beams, which is also the area where the beams are most prone to cracking. Cu-Al-Mn was the major component of the SMA fibers. To protect the cementitious material during the heating process, the austenite finish temperature was set at or near 100 °C. To assess the tensile flexural strength, a four-point bending test was carried out, and during the test, cracks appeared at the bottom of the beam. Subsequently, the SME was initiated, and the closed crack's width was assessed by employing a heating plate that could be affixed to the lower part of the beam. For various fiber volume fractions, specifically 0.25%, 0.5%, 0.75%, and 1%, the examination aimed to pinpoint the influence of SMA fibers on the beam's capacity to close cracks and their flexural tensile strength.

Many works focused on Cu-based SMAs involving economical materials such as Cu-Al-Mn, Cu-Zn-Al, Cu-Al-Ni, Cu-Al-Be-Mn, and Cu-Zn-Si [25,26]. Cu-Al-Be-Mn alloy possesses good mechanical characteristics, corrosion resistance, SE, and capacity to absorb vibration. Thus, it finds application in the petroleum industry for pipe joints because Be reduces phase transformation temperatures [27]. Candido et al**.** [28] conducted a comprehensive examination of a Cu-Al-Be alloy, wherein chromium (Cr) was introduced as a grain-refining agent. Their investigation encompassed both microstructural and mechanical assessments. Notably, the microscopic analyses unveiled a remarkable reduction in grain size, with values diminishing from 1950 to 100 μm for samples containing 0.5 wt.% Cr and those devoid of Cr (0 wt.%), respectively. One noteworthy outcome emerged when they evaluated the alloy containing 0.2 wt.% Cr. Hence, an increase in the Cr content in the Cu-Al-Be alloy leads to a more pronounced effect in grain refinement. This specific composition demonstrated enhanced tensile stress-strain characteristics. Additionally, it exhibited a notable reduction in Martensitic transformation temperatures. These findings suggest that this particular alloy composition may offer distinct advantages for applications involving low-temperature conditions. In a study by Prawdzik et al. [29], it was noted that the introduction of Be into the Cu-Al binary system led to a significant reduction in transformation temperatures, with some transformations occurring at or below room temperature. Concurrently, Higuchi et al. [30] examined the connection between element composition and transformation temperatures. The research revealed that the incorporation of 0.1 wt.% Be into the Cu-Al SMA resulted in a substantial decrease of approximately 100 °C in phase transformation temperatures. Oliveira et al. [31–33] explored the potential of Cu-based shape memory alloys, such as Cu-17Al-11.4Mn and Cu-Al-Be, as substitutes for NiTi due to lower costs and improved mechanical properties. The first study focused on Cu-17Al-11.4Mn, revealing enhanced ductility in the fusion zone and superior SE. The second study introduced post-weld laser processing, resulting in increased tensile strength and energy absorption for seismic applications. The third study investigated laser welding of single crystal-like Cu-Al-Be alloys, yielding defect-free joints with preserved SE behavior and high energy absorption, making them promising for damping applications in seismic systems. Overall, these studies advanced the understanding of weldability and mechanical properties, expanding the potential of Cu-based shape memory alloys in various engineering applications.

However, a few comprehensive studies on Cu-Al-Mn have been conducted to enhance mechanical properties and lower transformation temperatures. The primary objective of this study is to synthesize SMAs alloys of Cu-Al-Mn and Cu-Al-Be-Mn and study the chemical composition, transformation temperatures, and effect of fiber volume percentage on the mechanical properties of the composites reinforced with SMAs wires for specific engineering applications.

2. Materials and methods

This section discusses the synthesis of different SMA alloys of Cu-Al-Mn, and Cu-Al-Mn-Be with varied proportions of individual contents.

2.1. Casting of Cu-Al-Mn, Cu-Al-Be-Mn SMA

The research focused on Cu-based SMAs that contained varying compositions of Al (10–14.5 wt.%) and Mn (0–10 wt.%). These specific alloy compositions were selected to ensure the presence of the ß-phase and to observe the SME. Roughly 500 g of the alloy was melted in a crucible coated with graphite under an argon atmosphere using a resistance-heated furnace. Subsequently, the molten alloy was poured into a cast iron mold with dimensions of 0.15 × 0.10 × 0.006 m and allowed to cool and solidify.

To refine the resulting ingots, a homogenization process was carried out at a temperature of 1173 K, which falls within the ß-phase range. This process lasted for 21.6 kiloseconds and was conducted in an argon atmosphere. The exact compositions of the cast alloys were determined using an optically coupled plasma-optical emission spectrometer (OCP-OES). For a visual representation of the casting procedure employed in synthesizing the SMAs, please refer to Figure 1.

Cu-based SMAs were prepared by varying the content of Al-Mn and Al-Mn-Be, as indicated in Tables 1 and 2 respectively. The process involved melting 500 g of pure Cu, Al, and Be pieces for each specific alloy in an induction furnace. After melting, the molten alloy was poured into a cast iron mold with dimensions of 0.15 × 0.10 × 0.006 m and left to solidify. Subsequently, the resulting ingots underwent a homogenization process at 1173 K for a duration of 6 h. The alloy compositions were accurately determined using an OCP-OES. Figure 2 shows the overall experimental setup used in the casting of Cu-Al-Mn and Cu-Al-Be-Mn SMAs.

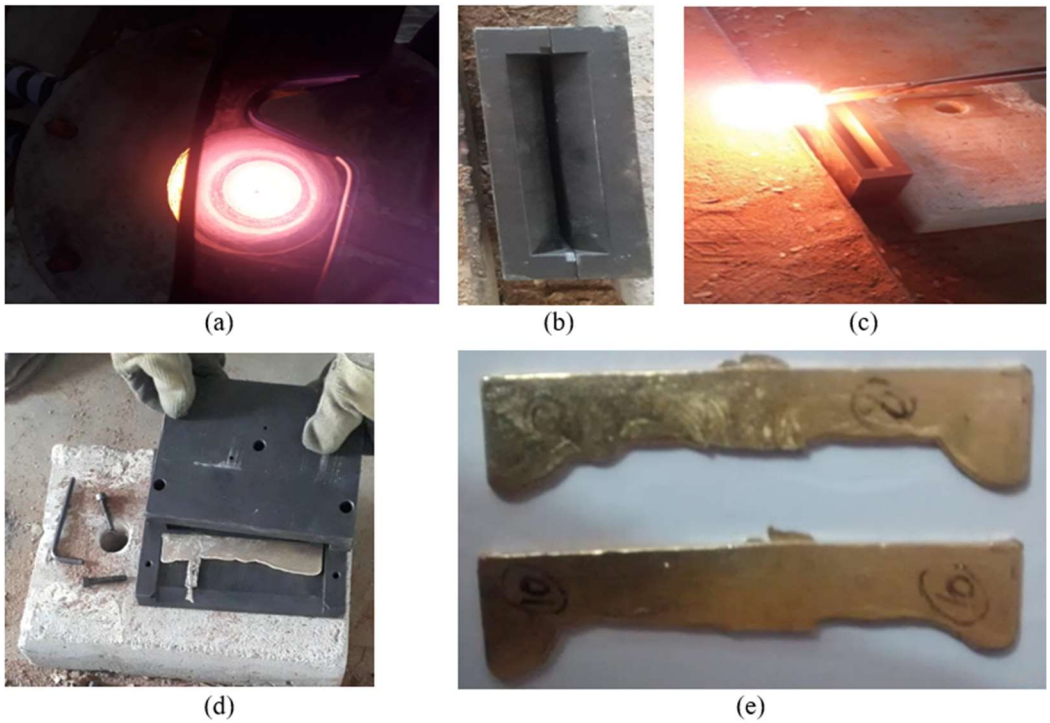

Figure 1. Casting process of SMA alloys.

Figure 2. Overall casting experimental setup.

Table 1. Chemical composition of Cu-Al-Mn SMAs.

Samples	Composition (wt.%)		
	Cu	Al	Mn
SMA 1	80.94	10.54	8.52
SMA 2	81.10	10.81	8.10
SMA 3	83.52	11.36	5.12

Table 2. Chemical composition of Cu-Al-Mn-Be SMAs.

Samples	Composition (wt.%)			
	Cu	Al	Be	Mn
SMA 4	88.38	11.0	0.42	0.2
SMA 5	87.85	11.5	0.45	0.3
SMA 6	87.42	11.8	0.48	0.3

2.2. Al metal matrix composites with SMA fibers reinforcement

Figure 3 shows the rolling, cutting and wire drawing machines used in the development of SMA fibers from Cu-Al-Mn and Cu-Al-Be-Mn combinations respectively.

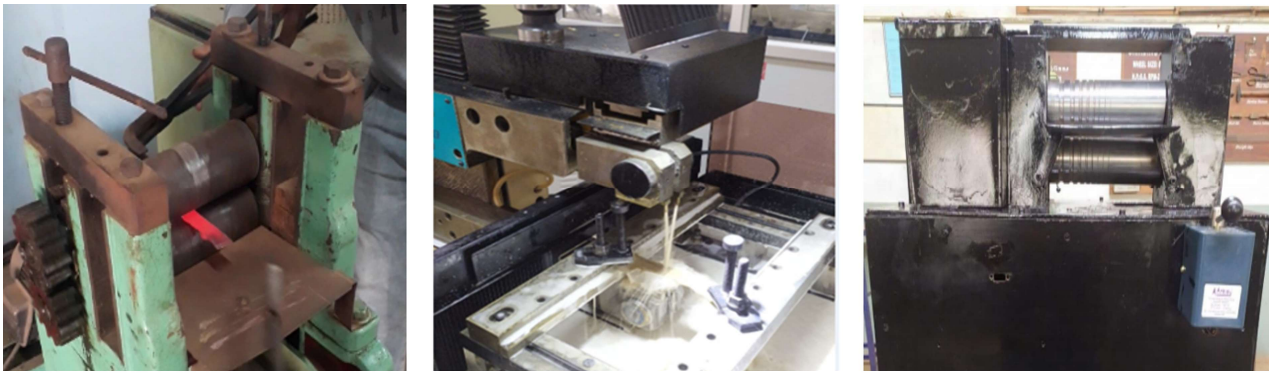

Rolling machine Wire cutting machine Wire drawing machine

Figure 3. SMA fiber synthesis.

Figure 4 shows the frame for holding SMA fibers in the form of wires with pre-tension and their subsequent reinforcement with the Al matrix. These wires reinforced with Al matrix were 0.8 mm in diameter.

Figure 4. Frame construction for holding wire for reinforcing with Al matrix.

2.3. Preparation of Al metal matrix composites

Figure 5 shows Al alloy reinforced with Cu-Al-Mn and Cu-Al-Be-Mn SMA fibers during fabrication of composites with reinforcement arrangement used. Figure 6a and 6b shows the synthesis of Cu-Al-Mn and Cu-Al-Be-Mn SMA alloys notched before and after the cracking sample and Figure 6c shows the schematic of reinforcement arrangement.

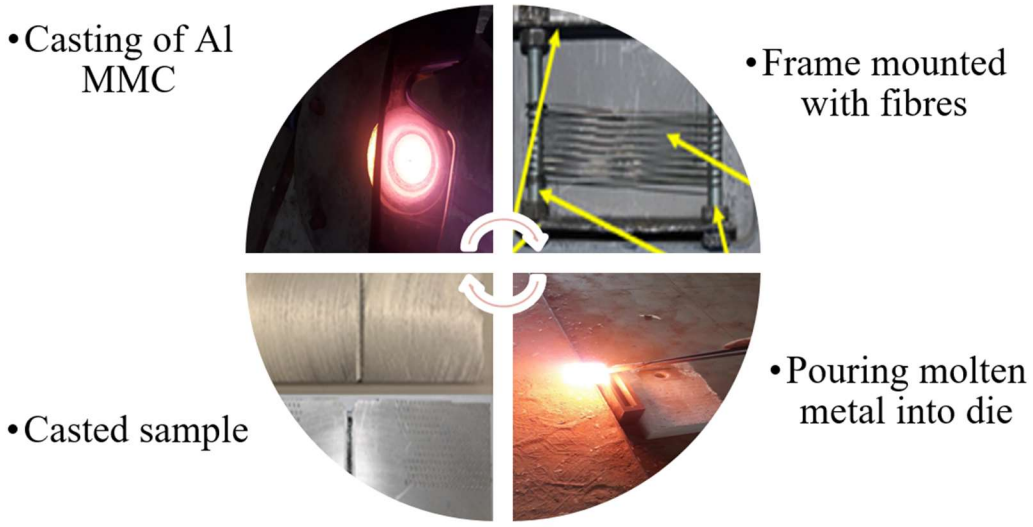

Figure 5. Preparation of Al metal matrix composites.

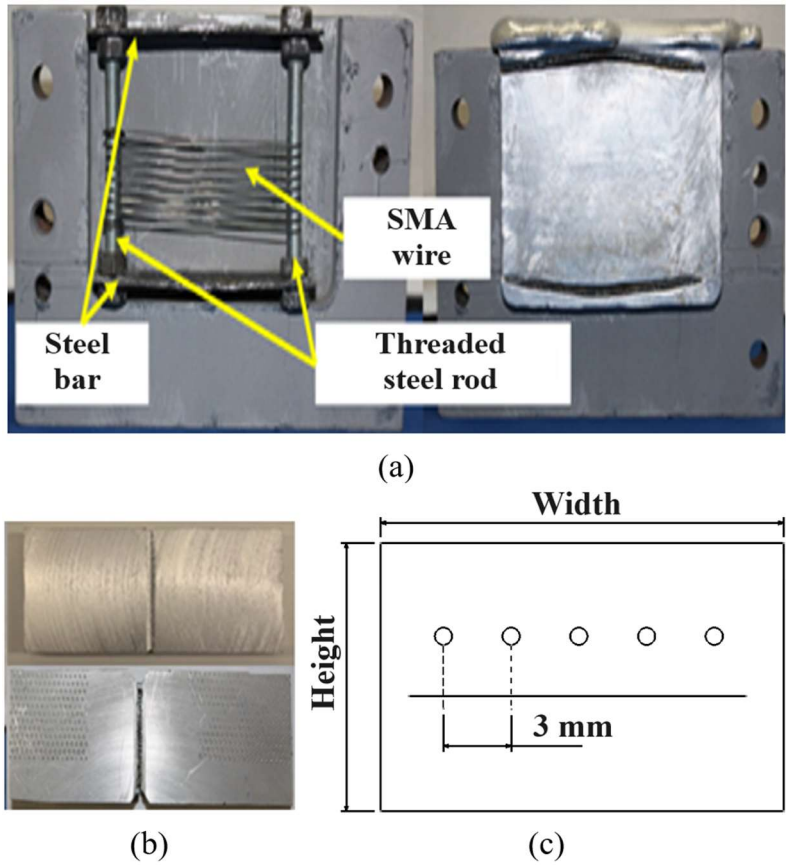

Figure 6. (a) Synthesis of Cu-Al-Mn and Cu-Al-Be-Mn SMA alloys, (b) notched SMA samples and (c) schematic of reinforcement arrangement.

3. Results and discussion

3.1. Effect of varying content of Al and Mn on the performance of Cu-Al-Mn SMAs

This section discusses the chemical composition, transformation temperatures, SME, and SE of Cu-Al-Mn SMAs with varied proportions of Al and Mn respectively. Table 3 shows Cu-Al-Mn-based SMAs with varied content of Cu, Al, and Mn respectively and their transformation temperatures (M_f—martensite finish, M_s—martensite start, A_s—austenite start and A_f—austenite finish). Among these SMAs, SMA 1 showed a lower transformation temperature compared to SMA 2 and SMA 3 respectively.

Table 3. Chemical composition and transformation temperature of SMAs alloys of Cu-Al-Mn.

Sample number	Composition (wt.%)			Transformation temperature (K)			
	Cu	Al	Mn	M_f	M_s	A_s	A_f
SMA 1	80.94	10.54	8.52	306	322	325	339
SMA 2	81.10	10.81	8.10	334	358	346	370
SMA 3	83.52	11.36	5.12	370	390	391	416

3.1.1. Effect of Al and Mn content on chemical composition, transformation temperatures of Cu-Al-Mn SMAs

In order to study the effect of Al content with Mn content fixed on the transformation temperature, two other SMAs (SMA 1N and SMA 2N) were developed as shown in Table 4. Keeping Al constant and increasing the Mn concentration decreases the transformation temperature and increases the strain recovery.

Table 4. Chemical composition and transformation temperature of SMAs alloys of Cu-Al-Mn with constant Al content.

Sample number	Composition (wt.%)			Transformation temperature (K)				Strain recovery (%)	SE (%)
	Cu	Al	Mn	M_f	M_s	A_s	A_f		
SMA 1N	80.94	12	7.06	282	299	304	319	79	8
SMA 2N	82	12	6.0	294	318	321	341	91	7
SMA 1	80.94	10.54	8.52	306	322	325	339	95	8
SMA 2	81.10	10.81	8.10	334	358	346	370	89	7
SMA 3	83.52	11.36	5.12	370	390	391	416	90	8

To further study the effect of varying Mn and constant Al on the transformation temperature, the new SMAs (SMA 3N and SMA 4N) were considered as shown in Table 5. Keeping Mn constant and reducing the Al increases the transformation temperature.

Table 5. Chemical composition and transformation temperature of SMAs alloys of Cu-Al-Mn with constant Mn content.

Sample number	Composition (wt.%)			Transformation temperature (K)				Strain recovery (%)	SE (%)
	Cu	Al	Mn	M_f	M_s	A_s	A_f		
SMA 3N	81	13	6	295	317	321	341	93	6
SMA 4N	83	11	6	322	346	342	368	89	7
SMA 1	80.94	10.54	8.52	306	322	325	339	95	8
SMA 2	81.10	10.81	8.10	334	358	346	370	89	7
SMA 3	83.52	11.36	5.12	370	390	391	416	90	8

3.1.2. Effect of Al and Mn content on SME and SE of Cu-Al-Mn SMAs

Figure 7a shows the photographic view of shape recovery determination for the SMAs synthesized. Shape memory strain recovery was determined for these SMA alloys as shown in Tables 6 and 7. Figure 7b shows the schematic view of shape recovery determination for the SMAs. The shape fixity (R_f) and the shape recovery (R_r) were evaluated with Eqs 1 and 2 respectively.

$$R_f = \frac{\epsilon_u}{\epsilon_m} \times 100\% \quad (1)$$

$$R_r = \frac{\epsilon_m - \epsilon_p(N)}{\epsilon_m - \epsilon_p(N-1)} \times 100\% \quad (2)$$

where ϵ_u is the original unloading strain, ϵ_m is the original maximum strain, and ϵ_p is the residual strain.

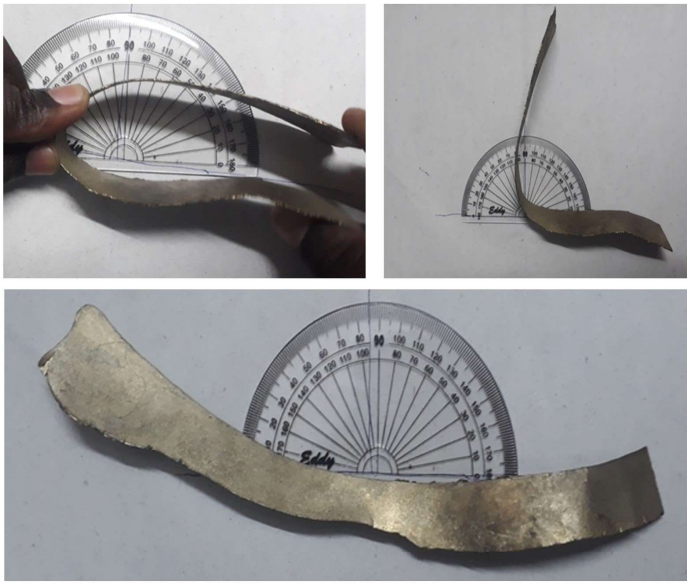

(a)

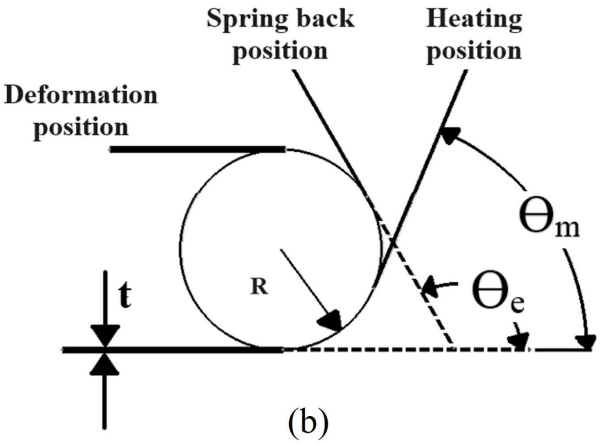

(b)

Figure 7. (a) Photographic view of shape recovery calculation. (b) Schematic view of shape recovery calculation.

From Table 6, it follows that for Cu-Al-Mn SMAs, SMA 1 showed higher strain recovery which increased by 6.74% and 5.55% compared to SMA 2 and SMA 3 respectively.

Table 6. Shape memory strain recovery in Cu-Al-Mn alloys.

Sample number	Strain recovery (%)
SMA 1	95
SMA 2	89
SMA 3	90

From Table 7 it follows that for Cu-Al-Be-Mn SMAs, the SMA 6 showed higher strain recovery which increased by 45.45% and 9.1% compared to SMA 4 and SMA 5 respectively.

Table 7. Shape memory strain recovery in Cu-Al-Be-Mn.

Sample number	Strain recovery (%)
SMA 4	66
SMA 5	88
SMA 6	96

The extent of strain recovery and SE of all the SMEs considered in the study is given in Table 8.

Table 8. SME and SE of Cu-Al-Mn SMAs.

Sample number	Strain recovery (%)	SE (%)
SMA 1N	79	8
SMA 2N	91	7
SMA 3N	94	5
SMA 4N	90	6
SMA 1	95	7
SMA 2	89	7
SMA 3	90	8

The SMAs have shown substantial strain recovery through the SME, ranging from 79%–95%. As indicated in Table 8, it can be observed that the composition of the alloy has little impact on strain recovery through SME, except for SMA 1N. The primary factor influencing strain recovery via SME is the extent of martensite-to-austenite transformation within the alloy system. The presence of any remaining martensite within the austenite phase of the alloy will proportionally reduce strain recovery [34]. Other variables, such as material imperfections like quenched-in vacancies and dislocations, affect strain recovery through SME. These imperfections cause the martensitic plates to be pinned, thereby impeding the transformation process and, consequently, strain recovery. Alloys with higher concentrations of Al and Mn exhibit greater strain recovery through SME. This may be attributed to the ease with which the transformation from martensite to austenite occurs, leading to lower transformation temperatures.

3.2. Cu-Al-Be-Mn SMA alloys

This section discusses the chemical composition, transformation temperatures, SME, and SE of Cu-Al-Be-Mn SMA alloys.

3.2.1. Chemical composition and transformation temperature of Cu-Al-Be-Mn SMA alloys

Chemical composition, transformation temperatures, SME, and SE of Cu-Al-Be-Mn SMAs are shown in Table 9 Among these SMAs, SMA 6 showed lower transformation temperature compared to

SMA 4 and SMA 5 with increasing content of Be and Mn respectively. The addition of Be content in Cu-Al-Mn SMAs showed comparatively lower transformation temperatures.

Table 9. Chemical composition and transformation temperature of SMAs alloys of Cu-Al-Be-Mn.

Sample number	Composition (wt.%)				Transformation temperature (K)			
	Cu	Al	Be	Mn	M_f	M_s	A_s	A_f
SMA 4	88.38	11.0	0.42	0.2	316	325	331	354
SMA 5	87.85	11.5	0.45	0.25	311	346	334	367
SMA 6	87.42	11.8	0.48	0.3	302	314	324	333

3.3. Mechanical properties of Cu-Al-Mn and Cu-Al-Be-Mn SMA alloys

This section discusses the testing of SMA-based composites to determine the mechanical properties such as residual strength, energy absorption capacity, cracking strength, and cracking widths respectively.

3.3.1. Residual strength or percentage of shape recovery (strains) of SMA alloys

Figures 8 and 9 illustrate the changes in residual strength in two types of SMAs: Cu-Al-Mn and Cu-Al-Be-Mn. These SMAs were infused with varying fiber volumes, ranging from 0–1.00%. Notably, the beams entrenched with SMA fibers exhibited an increase in residual flexural strength as the fiber volume fraction increased. This is in stark contrast to the control specimens lacking SMA fibers, which exhibited immediate deterioration after cracking.

The post-cracking residual strength remained intact in the SMA fiber-embedded beams, with only a minor reduction in flexural strength. Among the tested SMAs, SMA 1 displayed a higher residual strength due to the increased addition of Mn to the binary Cu-Al alloy. This addition stabilized the BCC phase, resulting in a lower temperature range for the existence of the β-phase. Consequently, this expanded the composition range, enhancing the alloy's ductility and reducing the degree of order [23,24].

Similar trends were observed in Cu-Al-Be-Mn SMA alloys, with SMA 6 demonstrating higher residual strength due to the increased incorporation of Be. Notably, Cu-Al-Be-Mn SMAs exhibited superior residual strength when compared to Cu-Al-Mn SMAs.

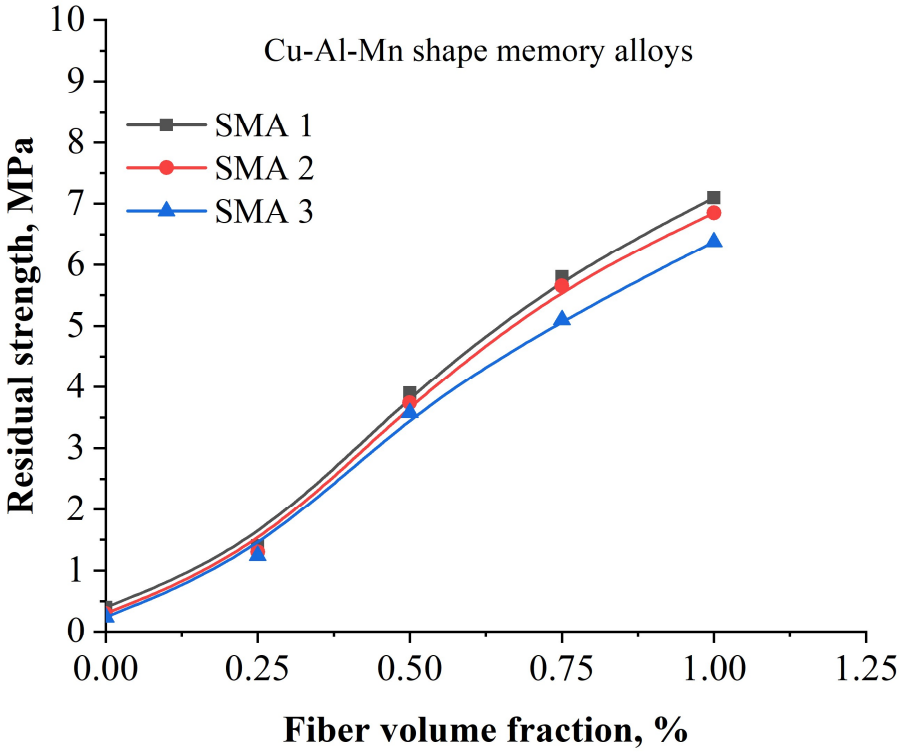

Figure 8. Variation of residual strength with fiber volume fraction of Cu-Al-Mn SMA alloys.

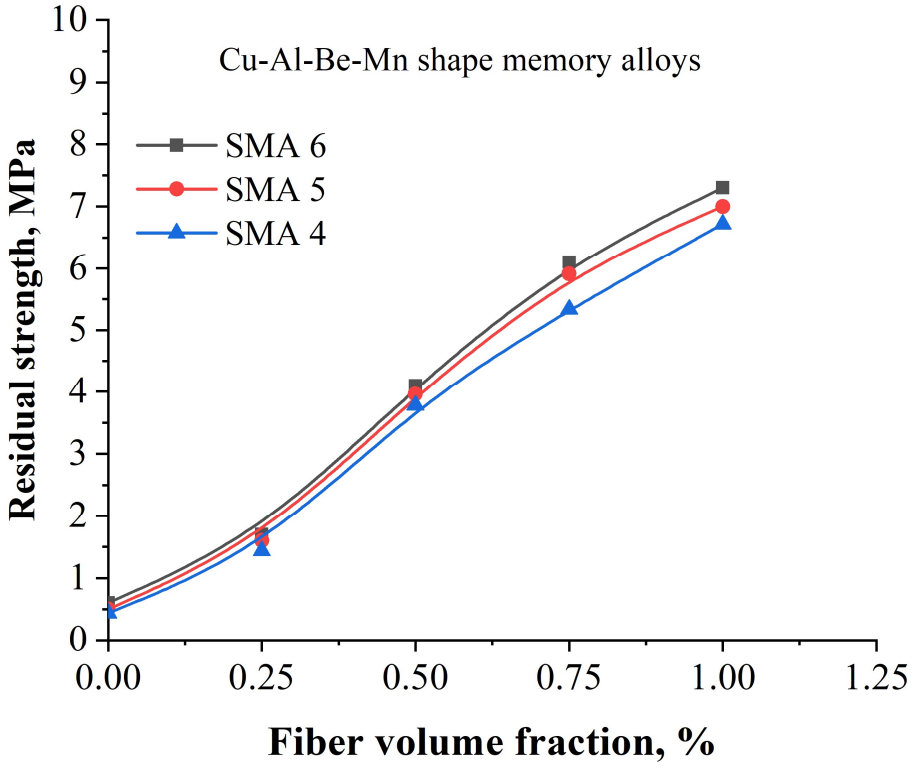

Figure 9. Variation of residual strength with fiber volume fraction of Cu-Al-Be-Mn SMA alloys.

3.3.2. Energy absorption capacity of SMA alloys

Figures 10 and 11 show variations in energy absorption capacity, which varies with fiber volume percentage. Energy absorption capacity can be determined by either analyzing the load and deflection data up to a specific point or by assessing the areas beneath the load and deflection curves. The former method is adopted in the present study.

A slight decrease in energy absorption capacity is obtained with a rise in fiber volume percentage which is consistent with SMA fibers having little effect on energy absorption capacity. SMA 1 showed higher energy absorption capacity compared to other coupons as a higher addition of Mn facilitates stability of disordered phase β. Hence, more energy is required for transformation [23,24]. Similar trends are observed with Cu-Al-Be-Mn SMA alloys where SMA 6 showed higher energy absorption capacity as higher addition of Be facilitates stability of disordered phase β as depicted in Figure 11. Cu-Al-Be-Mn SMA alloys showed higher energy absorption capacity compared to Cu-Al-Mn.

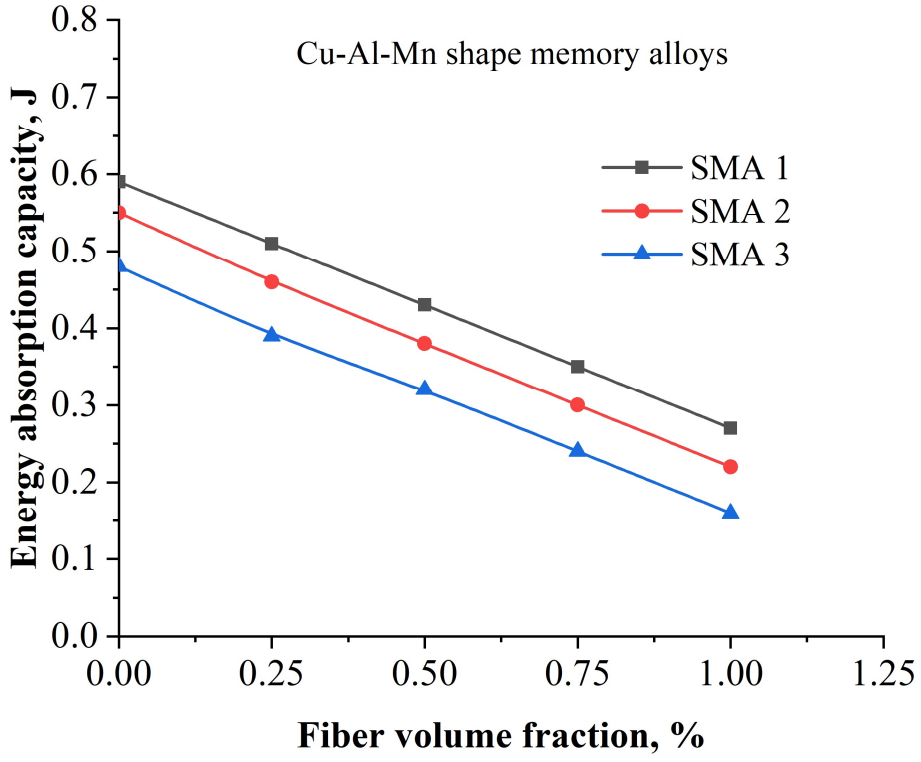

Figure 10. Variation of energy absorption capacity with fiber volume fraction of Cu-Al-Mn SMA alloys.

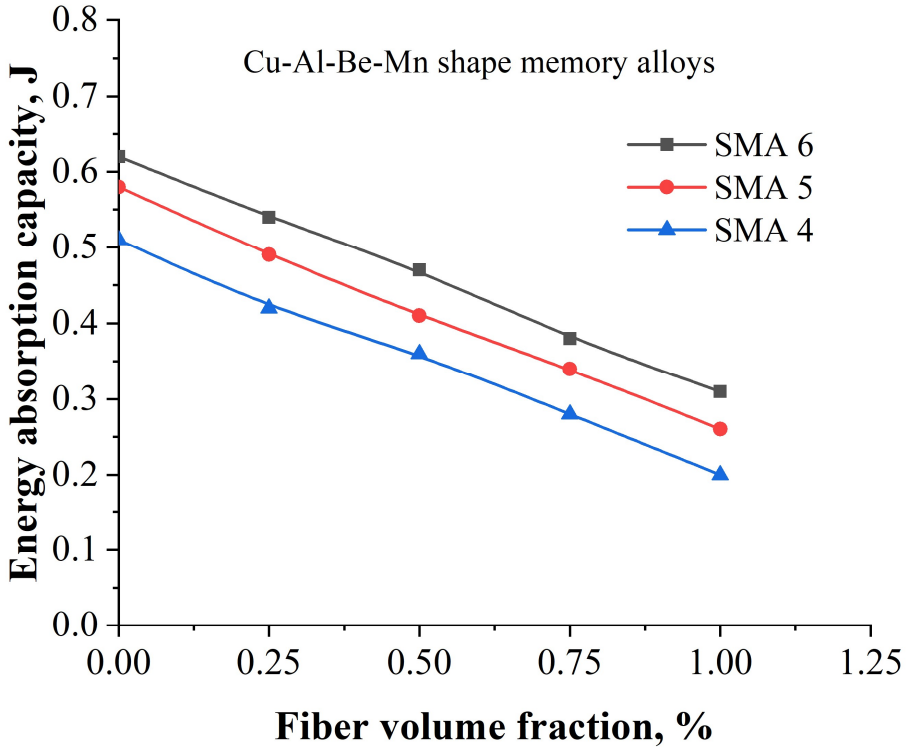

Figure 11. Variation of energy absorption capacity with fiber volume fraction of Cu-Al-Be-Mn SMA alloys.

3.3.3. Cracking strength of SMA alloys

Figures 12 and 13 show the correlation between cracking strength and fiber volume (%). During the bending tests, the initial occurrence of cracking took place in the lower section of the beam, with these cracks gradually propagating upward within the beam structure. Following a gradual reduction of the applied load on the beam, measurements were taken to assess the width of the flexural crack at the lower part of the structure. This involved the precise measurement of the crack's dimensions at five different points along its length, using a magnifying glass.

To address and seal the crack, a heating plate was employed. It was used to heat the SMA fibers inserted at the base of the beam to a temperature at least equal to the austenite finish temperature. The heating process continued until a thermocouple, attached to the central area of the beam's surface, reached the requisite temperature of 120 °C. Subsequently, post-cooling, the crack width was reevaluated to confirm that the closure had not led to any alteration in its dimensions.

As seen from Figure 12, SMA 1 exhibited comparatively higher cracking strength due to improved ductility provided by Mn addition thereby decreasing the degree of order [23,24]. Furthermore, as ductility increases, the energy required for crack propagation increases, and the resistance for crack propagation is enhanced.

Similar trends are observed with Cu-Al-Be-Mn SMA alloys where SMA 6 showed higher cracking strength due to improved ductility provided by Mn and Be addition thereby decreasing the degree of order as depicted in Figure 13. Cu-Al-Be-Mn SMA alloys showed higher cracking strength compared to Cu-Al-Mn.

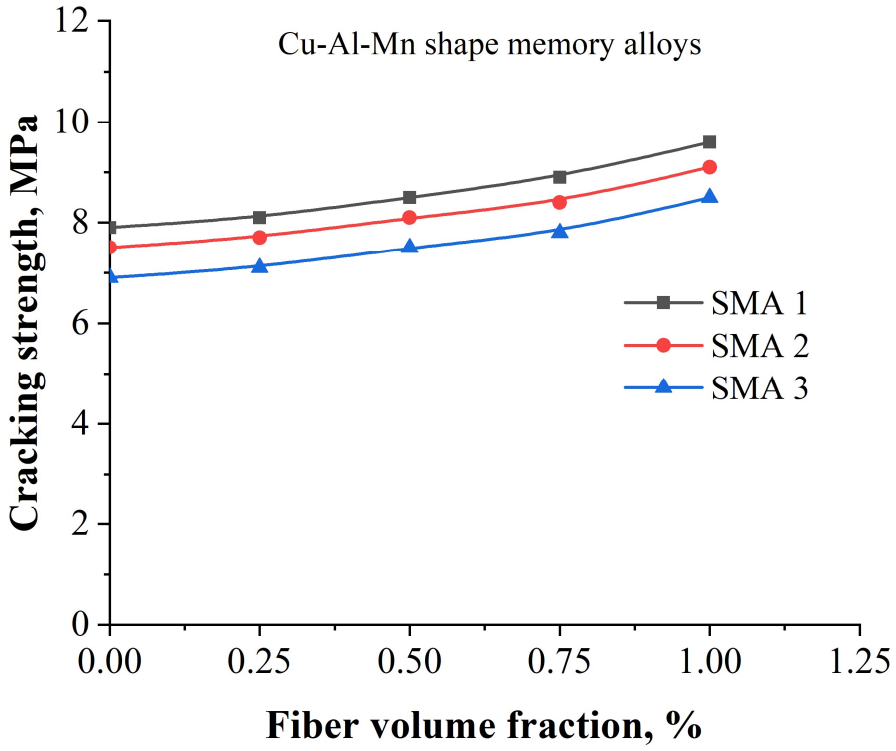

Figure 12. Variation of cracking strength with fiber volume fraction of Cu-Al-Mn SMA alloys.

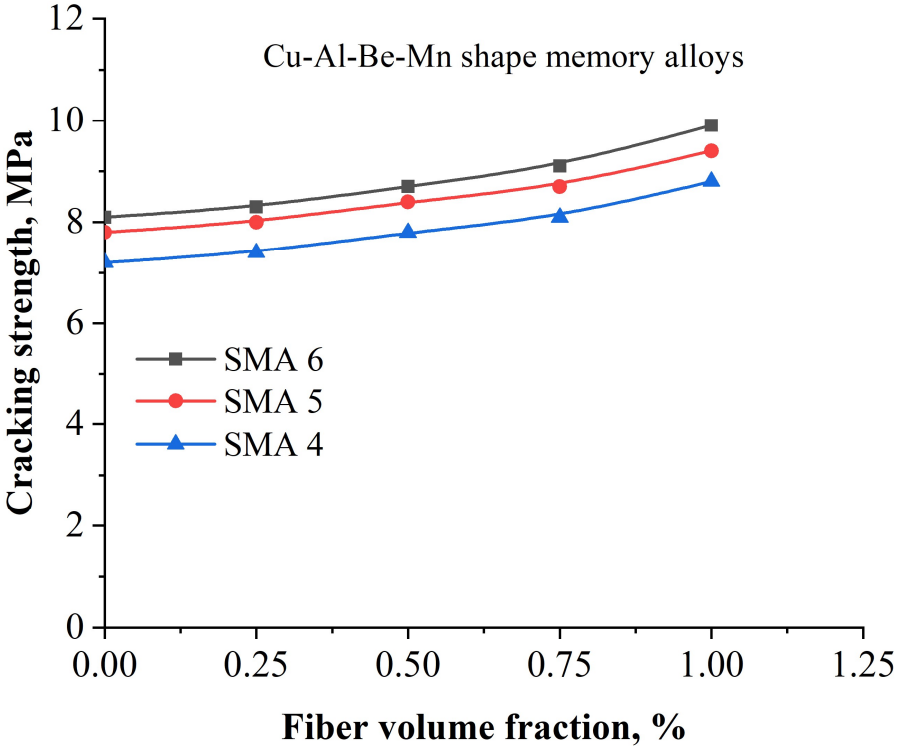

Figure 13. Variation of cracking strength with fiber volume fraction of Cu-Al-Be-Mn SMA alloys.

3.3.4. Crack widths of SMA alloys

In Figure 14, the measured crack widths are presented for both pre-heating and post-heating conditions. When compared to beams that lack tensile wires, the beams with embedded SMA fibers exhibit a more rapid reduction in crack width, indicating an enhanced capacity to close cracks. The effectiveness of crack closure in these beams improved by approximately 22%–28% when the SMA fiber content on the underside subjected to tensile forces ranged between 0.5% and 1%. Furthermore, an increase in the number of SMA fibers on the tensile underside of the beam specimens with tensile wires was observed to lead to a further enhancement in crack-closing performance. Notably, SMA 1 demonstrated narrower cracks in comparison to other tested specimens, both before and after heating. Specifically, SMA 1 exhibited a reduction in crack width by 18.98% and 21.66% before and after heating, respectively, when compared to SMA 3.

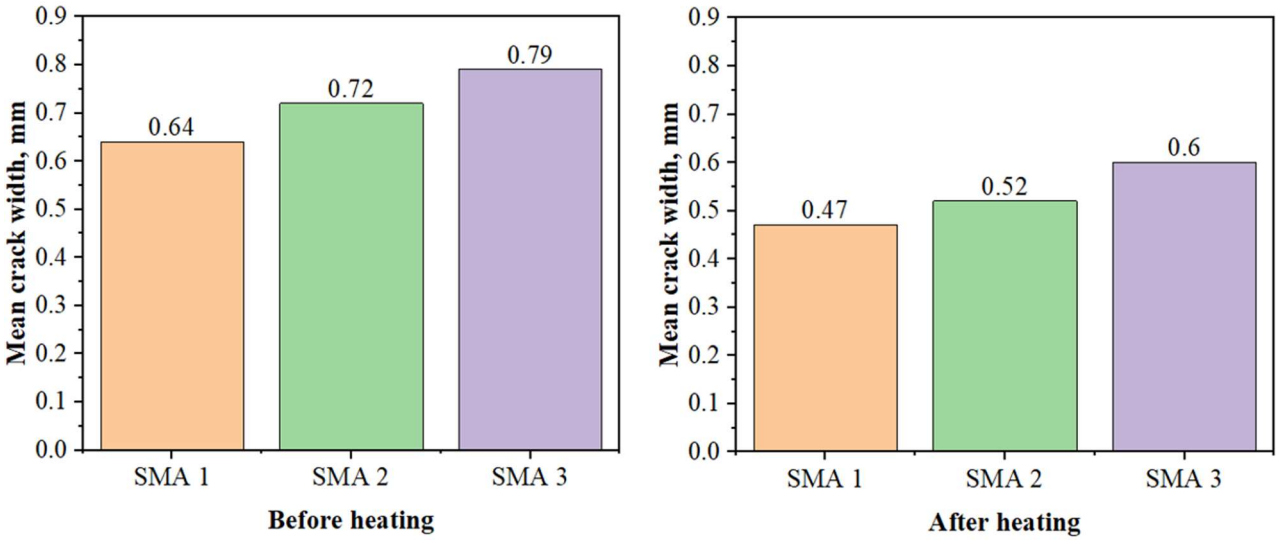

Figure 14. Variation of crack width for different SMAs.

4. Conclusions

This study focuses on the chemical composition, transformation temperatures, SME, and SE of Cu-Al-Mn and Cu-Al-Be-Mn SMAs respectively. Among the Cu-Al-Mn SMAs, SMA 1 showed higher strain recovery which increased by 6.74 % and 5.55 % compared to SMA 2 and SMA 3 respectively. Among the Cu-Al-Be-Mn SMAs, SMA 6 showed higher strain recovery which increased by 45.45% and 9.1% compared to SMA 4 and SMA 5 respectively.

Further, the mechanical properties of Cu-Al-Mn and Cu-Al-Be-Mn SMAs based Al MMC composites with varied percentages of SMA fibers are investigated.

The composite pour was only applied to the underside of the beam samples, a location more susceptible to cracking. The utilization of SMA fiber-infused composites was tested for their potential to seal fissures and impact the flexural tensile strength of the beams. During the four-point bending tests, the control beams exhibited a rapid decline in load resistance and a sudden, brittle failure. In contrast, the beams embedded with SMA fibers maintained load resistance even after experiencing

cracks. As a result of the bending tests, the bottom side of the beams displayed permanent flexural cracks. To address this, the SME of the SMA fibers positioned on the lower side of the beam was activated by heating, successfully closing the flexural cracks. Furthermore, it was observed that an increase in the quantity of SMA fiber on the tensile bottom side enhanced the crack-closure performance of the beam samples with tensile wires. However, the beams with tensile wires exhibited a moderate and consistent crack-closure ability, regardless of the specific types of SMA fibers employed.

Among the different SMAs synthesized, SMA 1 (Cu-80.94%, Al-10.54%, and Mn-8.52%) exhibited improved Martensite stability and SE compared to SMA 2 and SMA 3 respectively. SMA 1 showed higher residual strength, cracking strength, and energy absorption capacity compared to other selected coupons. At 1%, fiber volume fractions, SMA 1 showed higher residual strength (11.28%), energy absorption capacity (22.72%), cracking strength (12.94%), and lower crack widths (21.66%) compared to SMA 3 infused composite.

While among the Cu-Al-Be-Mn SMAs, the SMA 6 (Cu-87.42%, Al-11.8%, Be-0.48%, and Mn-0.3%) exhibited improved Martensite stability and SE compared to SMA 4 and SMA 5 respectively. SMA 6 showed higher residual strength, cracking strength, and energy absorption capacity compared to other selected coupons. At 1%, fiber volume fractions, SMA 6 showed higher residual strength (8.63%), energy absorption capacity (55%), and cracking strength (12.50%) compared to SMA 4 infused composite. Cu-Al-Be-Mn SMAs showed good mechanical properties compared to Cu-Al-Mn SMAs.

Use of AI tools declaration

The authors declare that they have not used Artificial Intelligence (AI) tools in the creation of this article.

Conflict of interest

The authors declare no conflict of interest.

References

1. Jani JM, Leary M, Subic A, et al. (2014) A review of shape memory alloy research, applications and opportunities. *Mater Design* 56: 1078–1113. https://doi.org/10.1016/j.matdes.2013.11.084
2. Torra V, Martorell F, Lovey FC, et al. (2017) Civil engineering applications: Specific properties of NiTi thick wires and their damping capabilities, a review. *Shap Mem Superelasticity* 3: 403–413. https://doi.org/10.1007/s40830-017-0135-y
3. Oliveira JP, Barbosa D, Fernandes FB, et al. (2016) Tungsten inert gas (TIG) welding of Ni-rich NiTi plates: Functional behavior. *Smart Mater Struct* 25: 03LT01. https://doi.org/10.1088/0964-1726/25/3/03LT01
4. Oliveira JP, Duarte JF, Inácio P, et al. (2017) Production of Al/NiTi composites by friction stir welding assisted by electrical current. *Mater Design* 113: 311–318. https://doi.org/10.1016/j.matdes.2016.10.038
5. Leonardo L, Antonio C (2014) *Shape Memory Alloy Engineering*, 1 Eds., Oxford: Butterworth-Heinemann. https://doi.org/10.1016/C2012-0-07151-7

6. Gao S, Yi S (2003) Experimental study on the anisotropic behavior of textured NiTi pseudoelastic shape memory alloys. *Mater Sci Eng A* 362: 107–111. https://doi.org/10.1016/S0921-5093(03)00585-9
7. Wang W, Fang C, Chen Y, et al. (2017) Innovative use of a shape memory alloy ring spring system for self-centering connections. *Eng Struct* 153: 503–515. https://doi.org/10.1016/j.engstruct.2017.10.039
8. Lu X, Zhang L, Lin K, et al. (2019) Improvement to composite frame systems for seismic and progressive collapse resistance. *Eng Struct* 186: 227–242. https://doi.org/10.1016/j.engstruct.2019.02.006
9. Li R, Ge H, Usami T, et al. (2017) A strain-based post-earthquake serviceability verification method for steel frame-typed bridge piers installed with seismic dampers. *J Earthq Eng* 21: 635–651. https://doi.org/10.1080/13632469.2016.1157531
10. Dolce M, Cardone D (2001) Mechanical behaviour of shape memory alloys elements for seismic applications: Part 1—Martensite and austenite NiTi bars subjected to torsion. *Int J Mech Sci* 43: 2631–2656. https://doi.org/10.1016/S0020-7403(01)00049-2
11. Dolce M, Cardone D (2001) Mechanical behaviour of shape memory alloys for seismic applications austenite NiTi wires subjected to tension. *Int J Mech Sci* 43: 2657–2677. https://doi.org/10.1016/S0020-7403(01)00050-9
12. Mekki OB, Auricchio F (2011) Performance evaluation of shape-memory-alloy superelastic behavior to control a stay cable in cable-stayed bridges. *Int J Nonlinear Mech* 46: 470–477. https://doi.org/10.1016/j.ijnonlinmec.2010.12.002
13. Torra V, Isalgue A, Auguet C, et al. (2011) SMA in mitigation of extreme loads in civil engineering: damping actions in stayed cables. *Appl Mech Mater* 82: 539–544. https://doi.org/10.4028/www.scientific.net/AMM.82.539
14. Zhang Y, Zhu S (2008) Seismic response control of building structures with superelastic shape memory alloy wire dampers. *J Eng Mech* 134: 240–251. https://doi.org/10.1061/(ASCE)0733-9399(2008)134:3(240)
15. Dieng L, Helbert G, Lecompte SA, et al. (2013) Use of shape memory alloys damper device to mitigate vibration amplitudes of bridge cables. *Eng Struct* 56: 1547–1556. https://doi.org/10.1016/j.engstruct.2013.07.018
16. Massah SR, Dorvar H (2014) Design and analysis of eccentrically braced steel frames with vertical links using shape memory alloys. *Smart Mater Struct* 23: 115015. https://doi.org/10.1088/0964-1726/23/11/115015
17. Yang CS, DesRoches W, Leon RT (2010) Design and analysis of braced frames with shape memory alloy and energy-absorbing hybrid devices. *Eng Struct* 32: 498–507. https://doi.org/10.1016/j.engstruct.2009.10.011
18. DesRoches R, Smith B (2004) Shape memory alloys in seismic resistant design and retrofit: A critical review of their potential and limitations. *J Earthq Eng* 8: 415–429. https://doi.org/10.1142/S1363246904001298
19. Wang Z, Xu L, Sun X, et al. (2017) Fatigue behavior of glass-fiber-reinforced epoxy composites embedded with shape memory alloy wires. *Compos Struct* 178: 311–319. https://doi.org/10.1016/j.compstruct.2017.07.027

20. Gholampour A, Ozbakkaloglu T (2018) Understanding the compressive behavior of shape memory alloy (SMA)-confined normal-and high-strength concrete. *Compos Struct* 202: 943–953. https://doi.org/10.1016/j.compstruct.2018.05.008
21. Pareek S, Suzuki Y, Araki Y, et al. (2018) Plastic hinge relocation in reinforced concrete beams using Cu-Al-Mn SMA bars. *Eng Struct* 175: 765–775. https://doi.org/10.1016/j.engstruct.2018.08.072
22. Abdulridha A, Palermo D (2017) Behaviour and modelling of hybrid SMA-steel reinforced concrete slender shear wall. *Eng Struct* 147: 77–89. https://doi.org/10.1016/j.engstruct.2017.04.058
23. Branco M, Gonçalves A, Guerreiro L, et al. (2014) Cyclic behavior of composite timber-masonry wall in quasi-dynamic conditions reinforced with superelastic damper. *Constr Build Mater* 52: 166–176. https://doi.org/10.1016/j.conbuildmat.2013.10.095
24. Shahverdi M, Michels J, Czaderski C, et al. (2018) Iron-based shape memory alloy strips for strengthening RC members: Material behavior and characterization. *Constr Build Mater* 173: 586–599. https://doi.org/10.1016/j.conbuildmat.2018.04.057
25. Kainuma R, Satoh N, Liu N, et al. (1998) Phase equilibria and Heusler phase stability in the Cu-rich portion of the Cu-Al-Mn system. *J Alloys Compd* 266: 191–200. https://doi.org/10.1016/S0925-8388(97)00425-8
26. Sutou Y, Kainuma R, Ishida K (1999) Effect of alloying elements on the shape memory properties of ductile Cu-Al-Mn alloys. *Mater Sci Eng A* 273: 375–379. https://doi.org/10.1016/S0921-5093(99)00301-9
27. Lara-Rodriguez GA, Gonzalez G, Flores-Zuniga GH, et al. (2006) The effect of rapid solidification and grain size on the transformation temperatures of Cu-Al-Be melt spun alloys. *Mater Charact* 57: 154–159. https://doi.org/10.1016/j.matchar.2005.12.017
28. Candido GVDM, Melo TADA, VHC De Albuquerque, et al. (2012) Characterization of a CuAlBe alloy with different Cr contents. *J Mater Eng Perform* 21: 2398–2406. https://doi.org/10.1007/s11665-012-0159-6
29. Prawdizg TJ, Zurey FT, Mack DJ, et al. (1966) An investigation of the mechanical properties and microstructures of heat treated aluminium bronzes.
30. Higuchi A, Suzuki K, Matsumoto Y, et al. (1982) Shape memory effect in Cu-Al-Be ternary alloys. *J Phys Colloques* 43: C4767–C4772. https://doi.org/ 10.1051/jphyscol:19824125
31. Oliveira JP, Panton B, Zeng Z, et al. (2016) Laser welded superelastic Cu-Al-Mn shape memory alloy wires. *Mater Design* 90: 122–128. https://doi.org/10.1016/j.matdes.2015.10.125
32. Oliveira JP, Zeng Z, Berveiller S, et al. (2016) Improvement of damping properties in laser processed superelastic Cu-Al-Mn shape memory alloys. *Mater Design* 98: 280–284. https://doi.org/10.1016/j.matdes.2016.03.032
33. Oliveira JP, Zeng Z, Berveiller S, et al. (2018) Laser welding of Cu-Al-Be shape memory alloys: Microstructure and mechanical properties. *Mater Design* 148: 145–152. https://doi.org/10.1016/j.matdes.2018.03.066

34. Morris MA, Lipe T (1994) Microstructural influence of Mn additions on thermoelastic and pseudoelastic properties of Cu Al Ni alloys. *Acta Metall Mater* 42: 1583–1594. https://doi.org/10.1016/0956-7151(94)90368-9